Water in nanopores. I. Coexistence curves from Gibbs ensemble Monte Carlo simulations

I. Brovchenko, A. Geiger, and A. Oleinikova
Physikalische Chemie, Universität Dortmund, D-44221 Dortmund, Germany

(Received 17 February 2003; accepted 15 October 2003)

Coexistence curves of water in cylindrical and slitlike nanopores of different size and water–substrate interaction strength were simulated in the Gibbs ensemble. The two-phase coexistence regions cover a wide range of pore filling level and temperature, including ambient temperature. Five different kinds of two-phase coexistence are observed. A single liquid–vapor coexistence is observed in hydrophobic and moderately hydrophilic pores. Surface transitions split from the main liquid–vapor coexistence region, when the water–substrate interaction becomes comparable or stronger than the water–water pair interaction. In this case prewetting, one and two layering transitions were observed. The critical temperature of the first layering transition decreases with strengthening water–substrate interaction towards the critical temperature expected for two-dimensional systems and is not sensitive to the variation of pore size and shape. Liquid–vapor phase transition in a pore with a wall which is already covered with two water layers is most typical for hydrophilic pores. The critical temperature of this transition is very sensitive to the pore size, in contrast to the liquid–vapor critical temperature in hydrophobic pores. The observed rich phase behavior of water in pores evidences that the knowledge of coexistence curves is of crucial importance for the analysis of experimental results and a prerequiste of meaningful simulations.
 [DOI: 10.1063/1.1631919]

I. INTRODUCTION

Fluids in confined geometries are presently an area of intense experimental and theoretical research and numerous computer simulations. Confined fluids are ubiquitous in nature and widely used in various industrial processes. Understanding the properties of confined fluids, which differ significantly from the properties of the bulk fluids, is of great fundamental and practical importance.

Considering the phase behavior of confined fluids, two typical situations may be distinguished: open pores and closed pores. In an open pore a confined fluid is in equilibrium with a saturated bulk liquid and may exist in a vapor or in a liquid one-phase state, which corresponds to capillary evaporation or capillary condensation, respectively. If there is no particle exchange with a bulk fluid (closed pore), the fluid in the pore may exist in a one-phase or a two-phase state, depending on temperature and average fluid density in the pore (level of pore filling).

The structural and dynamical properties of fluids are determined particularly by their density. Of course, the knowledge of an average density is not sufficient to predict the properties of a confined fluid, as it may exist in a one-phase or in a two-phase state. The spatial heterogeneity of a confined fluid may be caused not only by variations of the density due to the presence of the solid substrate but also by the coexistence of two phases of different densities. The interaction with the pore wall can lead also to the appearance of surface transitions (layering, wetting, prewetting etc.) and corresponding two-phase regions, which are marked by coexistence curves. So, at some arbitrary average fluid density in a pore various two-phases coexistences may be expected: liquid-vapor coexistence in a pore with a wall covered or not covered with liquid layers as well as coexistence of liquid and vapor layers near the pore wall. Obviously, the correct simulation of the structural and dynamical properties of a confined fluid needs the knowledge of its phase state, i.e. the number of coexisting phases (one, two, or even three in the case of a triple point), their densities and volume fractions at any given temperature and average density. This knowledge is also of crucial importance for the interpretation of experimental data on fluids in pores. Therefore, the study of the liquid–vapor coexistence curves of confined fluids is an urgent challenge.

In this paper we first analyze the current state of the experimental and theoretical research on liquid–vapor phase transitions in confined geometries and describe then in details techniques, which allow us to improve essentially the efficiency of the simulations of the coexistence curves. In the main part, the simulated coexistence curves of water in various nanopores are presented and briefly discussed. Whereas here our approach is to present in a more phenomenological way a systematic collection of coexistence curves, in subsequent papers a detailed analysis, based on available theories, will be presented.

A. Experimental studies of coexistence curves of fluids in pores

A sharp liquid–vapor phase transition was observed in various porous materials, whereas the experimental determination of full coexistence curves of fluids in pores is more difficult and only a few of them were constructed.[1–6] (Note

that a few so-called hysteresis coexistence curves, which show the temperature dependence of the extremes of the hysteresis loop, were also reported.[7,8])

The most accurate results were obtained by heat capacity and light scattering measurements for fluids in silica aerogels,[1,3] which have a wide distribution of pore sizes. For helium in aerogel an increase of the critical density (up to 17% with respect to the bulk value) and slight decrease of the critical temperature ($\Delta T_C = T_{3D} - T_C = 0.006 T_{3D}$, where T_{3D} is the bulk critical temperature) was observed accompanied by a strong narrowing of the two-phase region. This narrowing is much stronger at higher temperatures, giving rise to an unusual ''bottlelike'' shape of the coexistence curve in a wide temperature range.[1]

A few coexistence curves were estimated from adsorption measurements of fluids in porous glasses[4] and ordered mesoporous silica materials.[2,6] In this case a strong increase of the critical density (up to 100%) and a narrowing of the two-phases region was observed. Additionally, a few experimental estimates of pore critical temperatures only, based on adsorption measurements, were reported. The shifts of the critical temperature ΔT_C increased with decreasing pore size and $\Delta T_C = 0.30 T_{3D}$ to $0.35 T_{3D}$ was achieved in pores with radius $R_P = 12$ A.[9] Unfortunately, different methods to define the disappearance of the phase transition resulted in strongly differing values of ΔT_C for pores of similar size.[2,6,9]

Usually a pronounced adsorption–desorption hysteresis loop is observed when measuring adsorption in pores. This loop shrinks with increasing temperature and disappears at the hysteresis critical temperature T_{CH}. Hysteresis indicates nonequilibrium phase behavior due to the occurrence of metastable states. The microscopic origin of this phenomenon and its relation to the pore structure is still an area of discussion. In disordered porous systems hysteresis may be observed even without phase transition up to a hysteresis critical temperature $T_{CH} > T_C$, if the latter exists.[10] In single uniform pores T_{CH} is expected to be equal[11] or below[9,12] T_C. A number of experimentally determined T_{CH} values is available in the literature (see Refs. 6, 7, 9 and Ref. 13 for a data collection).

The experimental studies of the coexistence curves of fluids in porous materials which were presented above indicate essential changes of the critical parameters of fluids with respect to the bulk, but detailed studies are strongly limited by the available experimental techniques.

B. Theoretical background

Resuming the theoretical predictions for the effect of confinement in pores on fluid phase equilibria, it is reasonable to distinguish the role of three main factors: pore shape, pore size and fluid–substrate interaction.

1. Phase transitions in pores of various shape

The modification of phase diagrams was extensively studied theoretically for two main classes of porous media: single pores (slitlike and cylindrical) and disordered porous systems. In a slitlike pore there are true phase transitions and the liquid-vapor critical point belongs to the two-dimensional Ising universality class.[14,15] In a cylindrical pore the first order phase transitions are rounded. However, this rounding decreases exponentially with increasing cross-section area of the cylinder,[16] leading to rather sharp first-order phase transitions even in narrow pores.[11,17–19] Theory[20] and computer simulations[17,18,21,22] show that phase separation in a cylindrical pore appears as a series of alternating domains of two coexisting phases along the pore axis. Recent experiments[23] evidence the existence of phase-separated liquid domains of a fluid mixture confined in a porous glass. The characteristic length of these domains is related to the interfacial tension and increases exponentially with pore radius R_P and decreases exponentially with temperature.[20] At low temperatures it could be larger than 10^5 times the pore diameter even in very narrow pores.[21] A fluid confined in an infinite cylindrical pore is close to a one-dimensional system and thus it should not exhibit a true liquid–vapor critical point above zero temperature. However, a ''pseudocritical point'' could be defined as the temperature, when the surface tension between the domains of the two coexisting phases disappears. Above the pseudocritical point the alternating domain structure vanishes, and the fluid becomes homogeneous along the pore axis. It is still unclear, how the phase separation occurs in disordered pores: two phases coexist as alternating domains or as two infinite networks. A domain structure seems to be more probable in porous materials with low porosity. In highly porous materials, such as gels, infinite networks of two coexisting phases are usually assumed and the critical point of fluids in such random pores is expected to belong to the universality class of the random-field Ising model.[24]

2. Effect of pore size on phase transitions

The shift of the first-order phase transition of fluids confined in large pores is described by the Kelvin equation and in general is inversely proportional to the capillary size.[25] In cylindrical pores the shift of the phase transition is more significant than its rounding.[26] Density functional approaches predict a reduction of the critical temperature in narrow cylindrical and slitlike pores proportional to $1/R_P$ (or $1/H_P$, where H_P is width of a slitlike pore).[27,28] However, this approach is not valid close to the critical point, where the correlation length could be comparable to the pore size. In the critical range scaling theory predicts a reduction of the critical temperature $\Delta T_C = (T_{3D} - T_C) \sim H_P^{-1/\nu}$, where ν (≈ 0.63 for the Ising model), is the critical exponent, which describes the temperature dependence of the correlation length.[14,29] In the framework of the mean-field theory of critical phenomena, T_C is expected to decrease as $\Delta T_C \sim H_P^{-2}$.[29]

3. Effect of fluid–wall interaction on phase diagram

Analyzing the influence of a substrate on the fluid phase diagram, it is useful to distinguish two main factors, namely density variations of the fluid near the substrate and the appearance of surface transitions. Change of the fluid density and structure near the substrate distorts the liquid–vapor coexistence curve (both the critical parameters and the densities of the coexisting phases). This effect was studied in Refs. 14 and 29 and the critical temperature is predicted to be strongly influenced by the fluid–substrate interaction. Scaling theory

predicts that in a pore of fixed size the maximum shift of the critical temperature ΔT_C (at infinite fluid–substrate interaction) is 2.07 times larger than the minimum ΔT_C (at zero fluid-substrate interaction), compared to the mean-field value 2.60 of this ratio.[29] The critical density ρ_C is also shifted due to the fluid–substrate interaction. In the case of an attractive fluid–substrate interaction ρ_C averaged over the pore is higher than ρ_C of the bulk fluid, while in the central part of the pore the critical density appears to be below the bulk value.[14,29]

A more typical example of the surface influence on the fluid phase diagram is the appearance of various liquid–vapor surface transitions. A wetting transition appears ultimately at liquid–vapor coexistence in any semi-infinite fluid near a substrate.[30] It is connected with the formation of a thick macroscopic wetting layer in the vapor phase. If the wetting transition is a first-order phase transition, a so-called prewetting surface transition (transition between thin and thick films of fluid) could be observed away from the liquid–vapor coexistence.[31] At some strength of fluid–substrate interaction a layering transition occurs in undersaturated vapor near the surface. A layering transition is a surface transition, resulting in the formation of a single liquid monolayer on a substrate or on already adsorbed liquid layer(s).

In small pores, surface transitions influence the ''bulk'' liquid–vapor transition, which occurs in the pore interior, and, in turn, are affected by this shifted ''bulk'' liquid–vapor transition. Only for large pores, these two effects could be separated, while the narrowing of pores results in an increasing mixing of surface and ''bulk'' transitions.[32] Prewetting and layering transitions appear as additional coexistence curves, situated in the low density range due to the nonzero fraction of molecules participating in these transitions in pores. A density functional approach indicated that a prewetting transition could occur in slitlike and cylindrical pores.[28] With decreasing pore size the prewetting transition becomes unstable and eventually disappears. Sequences of layering transitions are truncated in pores, however, mean-field theory predicts that a finite number of layering transitions should survive even in a narrow pore.[33,34] These surface transitions should belong to the 2D universality class.[11,35] The presence of surface transitions results in a rich phase behavior of confined fluids, so several coexistence curves could be expected in the temperature-density plane.

The main (''bulk'') liquid–vapor coexistence curve of a fluid in a pore could be significantly distorted by surface transitions. Due to the presence of layering or prewetting transitions the liquid–vapor coexistence curve becomes narrower and the critical density is shifted to higher values with respect to the bulk. The formation of a wetting layer in a vapor phase along the liquid–vapor coexistence curve may distort its shape.[36] The special critical behavior in a surface layer[37] may also influence the shape of the liquid–vapor coexistence curve of a confined fluid. A so-called normal transition is expected in the surface layer of a semi-infinite fluid near the substrate.[38] The decrease of the local order parameter in a surface layer $\Delta\rho_1$ with increasing temperature should follow the power law $\Delta\rho_1 \sim (T - T_{3D})^{2-\alpha}$, where $\alpha \approx 0.1$ is a critical exponent. In magnetics a so-called ordinary transition is observed in the surface layer near the free surface.[37] In this case the local order parameter $\Delta\rho_1$ in the surface layer follows the power law $\Delta\rho_1 \sim (T - T_{3D})^{\beta_1}$, where the critical exponent $\beta_1 \approx 0.8$, which differs strongly from the value of the critical exponent $\beta \approx 0.326$ for the bulk coexistence curve. An ordinary transition should occur only if there is no preferential interaction of one of the phases with the substrate. In fluid systems this condition is almost unachievable. However, some experimental studies of binary fluids[39] (see also review in Ref. 40) and our simulations of a one-component fluid[41] show that the behavior of a fluid surface layer in the case of a weak surface field is similar to the one expected for an ordinary transition.

C. Coexistence curves of fluids in pores from computer simulations and theoretical approaches

Phase transitions in confined systems were extensively studied by various theoretical approaches (integral equation and density functional theories) and by computer simulations (molecular dynamics and Monte Carlo simulations).[42] However, coexistence curves of confined fluids were reported only in a few studies.

In a computer simulation an equilibrium phase transition can be located directly by equaling the chemical potentials, temperatures, and pressures in two coexisting phases. Both in computer simulations and theoretical approaches, phase transitions may also be located indirectly, by finding an equality of the grand thermodynamical potentials and chemical potentials of the two phases at fixed temperature (along the adsorption and desorption branches of isotherm).

The density functional theory is widely used to study phase transitions of confined fluids.[11,15,18,27,28,33,34,43–45] This approach allows to study both the shift of the bulk transition due to the confinement and various surface transitions, but with this method equilibrium phase transitions may be located only indirectly. Also, the density functional method intrinsically uses a mean-field approach, that ultimately results in a mean-field shape of the coexistence curve and in corresponding critical parameters. This feature is also characteristic for various other theoretical approaches which use a mean-field approximation.[46–48]

The limitations of the above-mentioned theoretical approaches in general may be avoided in computer simulations. Monte Carlo simulations in the grand canonical ensemble (GCMC) allow to obtain adsorption isotherms of fluids in various pores and to locate the equilibrium phase transition from the equality of the grand thermodynamical potential,[18,49–52] as already described above. Another method to locate equilibrium phase transitions based on adsorption isotherms was proposed recently.[53] It is based on the simulation of the complete isotherm, including unstable states and subsequent use of the Maxwell rule to locate the equilibrium phase transition. This method, however, is based on the assumption, that a small size of the simulation box provides homogeneity of a fluid in an unstable state. GCMC simulations may also be used to locate a phase transition by a histogram-reweighting method.[54,55] To obtain the coexisting densities in the GCMC ensemble, extended simulations are necessary to achieve a reasonable accuracy. That is why only

a few coexistence curves of confined fluids with only a few temperature points were obtained in such a way.

A direct equilibration of two coexisting phases may be obtained by simulation of both phases in one box (with explicit interface) or in two boxes (without interface). The first way seems to be the simplest at first glance. The densities of the coexisting phases could be defined as average densities of the phases far from the interface, or from block density distributions[56] at various temperatures and averaged densities. The density distribution shows a single maximum if the fluid is in a one-phase state or two maxima, if two-phase coexistence occurs. The main limitation of this method is the necessity to use an extremely large system size and the presence of interfaces. This drastically extends the time needed for the simulations. Therefore, this method was not widely applied (for the single example see Ref. 18).

Another direct method to simulate the coexistence curve of a confined fluid is the Gibbs ensemble Monte Carlo (GEMC) simulation.[57–60] In this ensemble, two phases are present in two separate simulation cells and phase coexistence is achieved without interface. The main difficulty of the GEMC method is the necessity to provide an essential number of molecular transfers between the simulation cells. Besides, equilibration of the pressure in the two cells requires a continuous variation of the cell volume, while preserving periodic boundary conditions. This means, that simulations in the GEMC are restricted to pores of simple geometry and smooth fluid–substrate potential. (Application of the GEMC to random porous media[59] contradicts the application of periodic boundaries.)

The presently available coexistence curves of confined one-component fluids with continuous interaction potentials, obtained from theoretical approaches and computer simulations, allow the conclusions, that the critical temperature of confined fluids decreases with decreasing pore size and strengthening fluid–substrate interaction. However, the available simulation data are not sufficient for a quantitative analysis and test of the theoretical predictions. The only attempt to analyze the shift of T_C caused by the confinement of a continuous fluid[58] suffers from a low accuracy of the data and an inappropriate way to estimate T_C. A shift of the critical density and narrowing of the two-phase region due to the confinement is usually observed. However, the origin of these effects (the influence of surface transitions, a specific critical behavior of surface layers, density variations near the pore wall, or simply ambiguities in the definition of the average fluid density in pores) remains unclear. The shape of the coexistence curves of liquid–vapor transitions, as well as layering and prewetting transitions of confined fluids were not analyzed yet, with the exception of a recent study of a fluid in a narrow slitlike pore (Ref. 55).

The goal of our study is to analyze in a systematic way the influence of pore size, shape, and fluid–substrate interaction on the fluid coexistence curves in pores of simple geometry and smooth fluid–substrate interaction. We intend to study layering and prewetting transitions (their appearance, their critical parameters and the shape of the coexistence curve), to analyze the shape of the liquid–vapor coexistence curve (influence of the formation of wetting layers and specific critical behavior in surface layers), to check theoretical predictions for the shift of the critical parameters due to the confinement. Such an analysis requires detailed knowledge of the coexistence curves, obtained by appropriate methods. In the present paper we report the coexistence curves of water in various pores, obtained by GEMC simulations. A detailed analysis of the influence of confinement and surface effects on the coexistence curves will be given in our next paper.

II. SIMULATION METHODS

TIP4P water[61] was simulated in cylindrical pores with radii R_P from 12 to 20 A and in slitlike pores of width $H_P = 24$ A. A spherical cutoff of 12 A (oxygen–oxygen distance) for both the Coulombic and Lennard-Jones (LJ) parts of the water–water interaction was used. In accord with the original parametrization of the TIP4P model, no long-range corrections were included. The interaction between the water molecules and the substrate was described by a (9-3) LJ potential:

$$U_{w\text{-}s}(r) = \varepsilon[(\sigma/r)^9 - (\sigma/r)^3], \tag{1}$$

where r is the distance from the water oxygen to the pore wall. The parameter σ was fixed at 2.5 A, whereas the parameter ε varied in order to change the well-depth U_0 of the potential (2) from -0.385 to -7.70 kcal/mol. The average water density in the pore was calculated, assuming that the water occupies a pore volume until the distance $\sigma/2 = 1.25$ A from the pore wall.

In the simulations of bulk TIP4P water a spherical cutoff of 8.5 A for the intermolecular interactions and long-range corrections for the LJ interactions were used.

A. Molecular transfers in the GEMC simulation

A MC simulation in the Gibbs ensemble[57,62] allows to achieve direct equilibration between two coexisting phases. These are simulated at a given temperature simultaneously in two simulation cells. Equality of the chemical potentials in both phases is achieved by periodic transfers of molecules from one box to the other one. A low probability of successful molecular transfers between the two coexisting phases is the main problem in GEMC simulations; this determines the limits of its applicability. The problem of molecular transfers increases sharply with increasing density, lowering temperature and due to highly orientated interactions like hydrogen bonding in water. Below we consider this problem, using the calculation of the chemical potential of bulk liquid water at ambient conditions as an example.

The energy distributions $p_0(U)$ of water molecules in liquid water at $T = 300$ K and $\rho = 1\ \mathrm{g\,cm^{-3}}$ and $p_1(U)$ of water molecules, randomly inserted in liquid water at the same conditions (5×10^8 insertions), are shown in Fig. 1 [curves p_0 and p_1(a)]. Only 4.8% of the randomly inserted molecules have energies $U < 40$ kcal/mol. The excess chemical potential μ_{ex} of the water molecules may be determined from these distributions using the overlapping distribution method[63,64]

$$\mu_{\mathrm{ex}} = U + kT \ln(p_0(U)/p_1(U)), \tag{2}$$

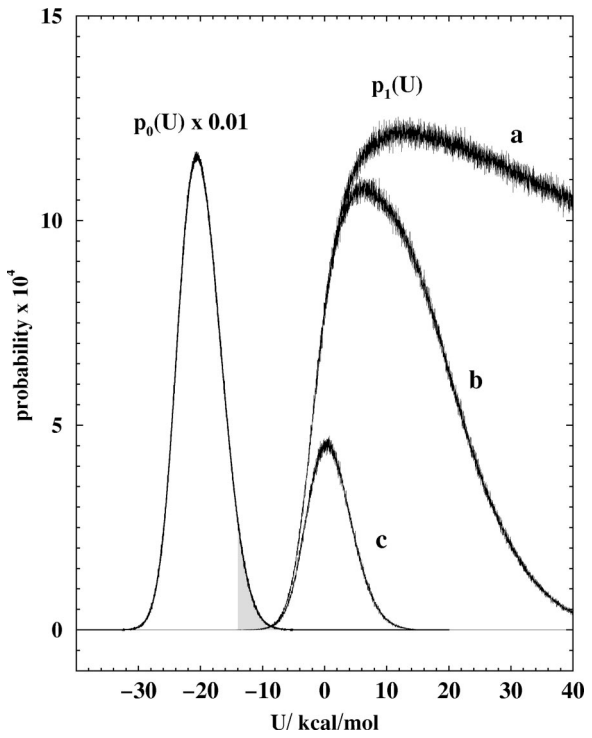

FIG. 1. Energetic probability distribution p_0 for molecules in liquid water at $T=300$ K and $\rho=1$ g/cm^3. Energetic probability distributions p_1 for molecules randomly inserted in liquid water at the same conditions: (a) total distribution; (b) distribution for molecules with criterium I for shortest interatomic distances; (c) distribution for molecules with criterium II for shortest interatomic distances. See text for the details.

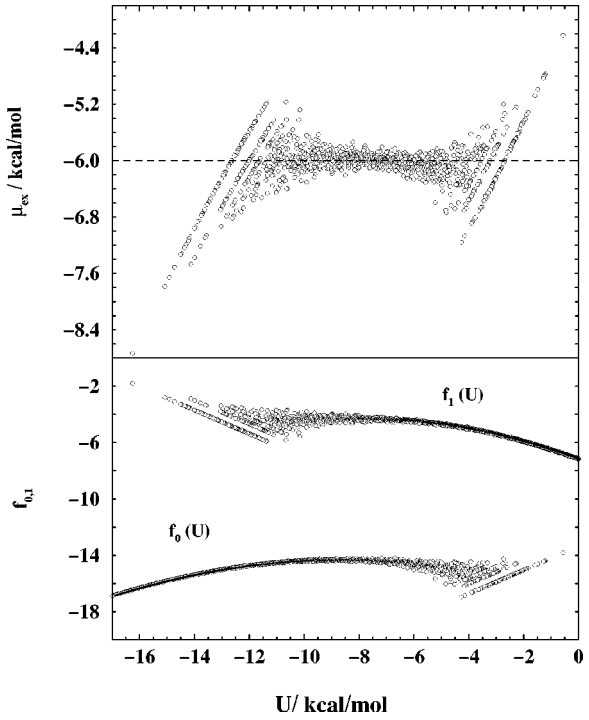

FIG. 2. Estimation of the excess chemical potential μ_{ex} of liquid TIP4P water by the overlapping distribution method. Lower panel, particle insertion $f_1(U)$ and particle deletion $f_0(U)$ functions. Top panel, fitting $\mu_{ex}(U)$ by Eq. (3) (dashed line). $\mu_{ex}=-6.00\pm0.08$ kcal/mol in the interval -9 kcal/mol$<U<-6$ kcal/mol.

or, defining a particle insertion function $f_1(U)=\ln(p_1(U))-U/2kT$ and a particle deletion function $f_0(U)=\ln(p_0(U))+U/2kT$,

$$\mu_{ex}=kT(f_0(U)-f_1(U)). \tag{3}$$

The accuracy of the obtained value μ_{ex} depends on the energy interval, where both functions may be determined. Although nonzero values of both $f_0(U)$ and $f_1(U)$ distributions were found in the range -15 kcal/mol$<U<0$ kcal/mol (Fig. 2), the statistically important interval of overlapping distributions is about -9.0 kcal/mol$<U<-6.0$ kcal/mol. Fitting of the data to Eq. (2) in this interval gives the value $\mu_{ex}=-6.00\pm0.08$ kcal/mol (Fig. 2, top panel, dashed line). This value is in a good agreement with available simulation results for the chemical potential of TIP4P water at the same temperature, obtained by other methods (-5.9 kcal/mol,[65] -6.06 kcal/mol,[66] -6.2 kcal/mol,[67] -5.97 kcal/mol,[68] -6.02 kcal/mol,[69] -6.11 kcal/mol[70]).

Random selection of a molecule in the dense liquid phase for removal results in numerous unsuccessful attempts to transfer it into the other phase: on average the molecule had a low energy in the initial box, whereas the probability to obtain a comparable energy after its insertion is negligibly small (see the tiny overlap in Fig. 1). Choosing highly energetic molecules for deletion (for example, molecules with energies, exceeding some critical value U_C, see shadowed area in Fig. 1) may improve the probability of a successful transfer. Such a choice is not random and the acceptance probability of the molecular transfer must be corrected by multiplying with a correction factor, which is equal to the probability to find at random a molecule with an energy $U>U_C$. This correction factor may be obtained from the full probability distribution $p_0(U)$. As this distribution depends on the water density, which is not constant during a GEMC simulation, a density dependent correction factor (within intervals of 0.01 g cm^{-3}) was calculated as running average in the course of the simulation. At temperatures around 300 K and $U_C=-14$ to -12 kcal/mol, the value of the correction factor for liquid water is about 0.01. Despite the low value of the correction factor and the necessity to calculate the energetic probability distribution, this technique improved the efficiency of molecular transfers at temperatures below 350 K essentially. At higher temperatures the use of this technique did not improve the efficiency of the molecular transfers and had no noticeable effect on the results.

When attempting a molecular insertion, at first, the shortest interatomic distances (R_S^{O-O}, R_S^{O-H}, and R_S^{H-H}) between the atoms of the inserted molecule and the atoms of the nearest molecules were calculated. If at least one of these distances is shorter than some chosen cutoff value (R_C^{O-O}, R_C^{O-H}, and R_C^{H-H}), the new configuration is rejected immediately without further calculations. This procedure in principle also requires a correction of the acceptance probability of a new configuration by a correction factor, which depends on the probability to find at random a proper configuration. In liquid water at a temperature of about 300 K configurations with $R_S^{O-O}<2.35$ A, $R_S^{O-H}<1.40$ A, or $R_S^{H-H}<1.30$ A (criterium I) are never observed in equilibrated systems during

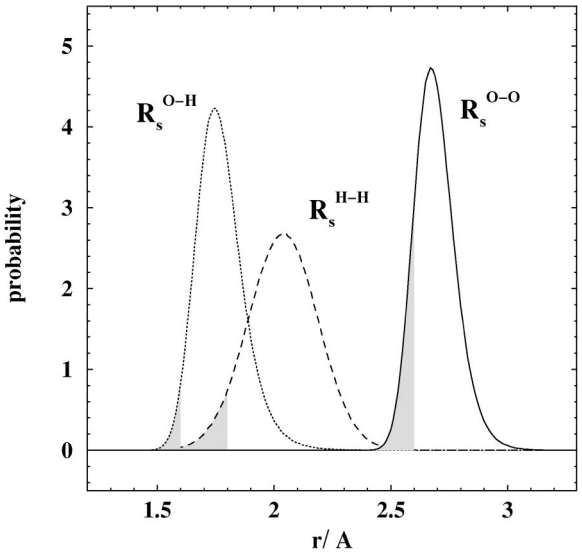

FIG. 3. Probability distribution of the shortest interatomic distances R_S^{O-O}, R_S^{O-H}, and R_S^{H-H} between a water molecule and its nearest neighbors in bulk water. $T=300$ K, $\rho=1$ g/cm^3. The shadowed areas denote configurations, which are excluded from molecular insertion attempts by criterium II.

long-term MC simulations (see Fig. 3) and so using criterium I for the rejection of a new configuration does not require a correction of the acceptance probability. The energetic probability distribution for molecules inserted in liquid water using criterium I, is shown in Fig. 1, curve p (b). Application of criterium I reduces the number of configurations, which demand energetic calculations, to 2.75% of the initial value and has no effect on the value of μ_{ex} obtained by the overlapping distribution method.

A further increase of the critical distances allows to reduce essentially the energy calculations. The interatomic cutoff distances $R_C^{O-O}=2.60$ A, $R_C^{O-H}=1.60$ A, and $R_C^{H-H}=1.80$ A (criterium II), used in the present simulations, were chosen empirically and are shown in Fig. 3. The energetic probability distribution for molecules, inserted by using criterium II, is shown in Fig. 1, curve p_1 (c). Application of criterium II reduces the number of configurations, which demand energy calculations, to 0.43% of the initial number. The value of $\mu_{ex}=-5.86\pm0.08$ kcal/mol, obtained by the overlapping distribution method with criterium II, is slightly depressed compared to the correct value $\mu_{ex}=-6.00\pm0.08$ kcal/mol. To restore the correct value μ_{ex}, in a first approximation the energetic probability p_0 has to be multiplied by a correction factor equal to the fraction of molecules in liquid water, which satisfy the chosen criterium for shortest interatomic distances. Use of criterium II gives the correction factor 0.85, which restores the correct value $\mu_{ex}=-6.02\pm0.08$ kcal/mol. Note, that such an approach is valid only when the statistically important high-energy tail of the energetic probability distribution p_0 may be restored by a single correction factor, and it may fail for larger interatomic cutoff distances. In the GEMC simulations running averages for different water densities (with steps of 0.01 g/cm^3) were used to increase the accuracy of the correction factor for the insertion. This technique allowed to improve noticeably the efficiency of the GEMC simulations at temperatures essentially below 300 K.

A molecular transfer in the GEMC simulations comprises deletion of a molecule in one box and its simultaneous insertion in the other box. Combination of the techniques, described above, allows to increase essentially the number of successful transfers. This provides much faster equilibration of the system and allows to study low-temperature and high-density regions.

B. Determination of the coexistence curves of water by GEMC simulations

As the densities of the coexisting phases may differ essentially (especially at low temperatures), their initial volumes were chosen to have a sufficiently large number of molecules in both phases to obtain reliable results. The minimal pore volume used for the liquid phase corresponds to a cylindrical pore with the length $2R_P$ and to a slitlike pore with an extension equal to the width H_P in the periodically continued directions. Thus, the length of the narrow cylindrical pores with water vapor attains extremely large values at low temperatures and approaches the length of the pore with the coexisting liquid phase (of about 10^2 A) at higher temperatures. The total number of water molecules in the two simulation cells varied from 400 molecules in the smallest pore to 2700 in the largest one. The minimal number of water molecules in the vapor phase was about 10 to 30 at low temperatures. For the simulation of bulk water the number of molecules in the vapor phase varied from 50 to 200 molecules, and in the liquid phase from 200 to 350 molecules.

Equality of the pressures in both phases is achieved by random changes of the volumes of the simulation boxes. This procedure can be easily implemented in the case of cylindrical and slitlike pores with smooth water–pore interaction. The maximal possible change of the pore volume was chosen to provide an acceptance probability of such moves of about 40% to 50%.

One GEMC simulation step contains 500 to 2000 attempts to displace and rotate molecules in each simulation cell with an acceptance probability of about 40% to 50%, one to two attempts to change the volumes with an acceptance probability of 40% to 50% and a series of N_{tr} attempts to transfer molecules between the two simulation cells with a probability of 10% to 30% for a successful transfer within this series. N_{tr} varied from only a few attempts to more than 10^6 attempts, depending on temperature and pore parameters. Typically from 10^4 to 10^5 steps were necessary in a GEMC simulation to get equilibrium between the two phases and a similar number of steps was used to collect the data and to obtain the densities of the coexisting phases. The total number of successful transfers was typically about $10N$, varying from $2N$ in large pores and low temperatures to $100N$ in small pores and high temperatures, where N is a total number of molecules in the two simulation cells.

An advantage of the GEMC method is the fact that the simulations may be started without knowledge of the densities of the coexisting phases. Using vaporlike and liquidlike bulk water densities is a natural choice for the initial con-

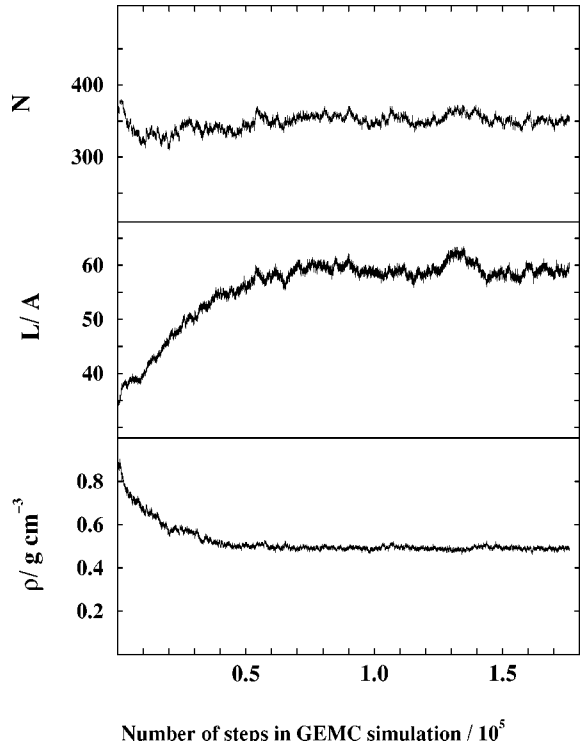

FIG. 4. Variation of the number of molecules, pore length and density of the liquid phase in the course of a Gibbs ensemble simulation. $T=300$ K, $R_P=12$ A, $U_0=-4.62$ kcal/mol.

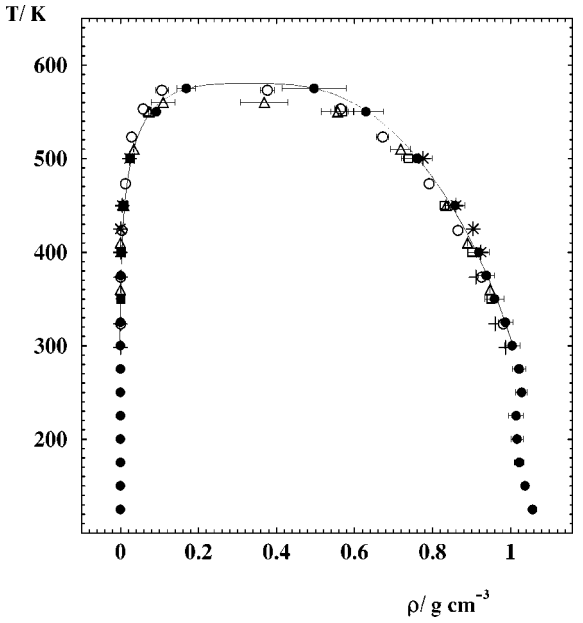

FIG. 5. Liquid–vapor coexistence curve of bulk TIP4P water. Closed circles, our results; stars, Ref. 71; crosses, Ref. 72; triangles, Ref. 73; open circles, Ref. 74; squares, Ref. 75. The line is a fit of our coexistence curve to Eqs. (4) and (5).

figurations. To locate the two-phase regions in the temperature-density plane, for a given temperature several average water densities of the total system were used as a starting point. A typical density variation during the equilibration process in the GEMC simulation is shown in Fig. 4. In some cases during the equilibration process the average density was adjusted (by changing the total pore volume) to have a sufficient number of molecules in both phases. When approaching the critical temperature, the density interval between the two phases shrinks, and therefore several values of the average density in the two cells were used in independent simulation runs to locate the coexistence or to prove its disappearance.

Close to the critical temperature, the fluids in the two simulation cells may start to exchange their identities. In such a case, phase separation may take place within one or both cells, which results in the formation of long-lived interfaces. This effect is especially pronounced in lengthy cylindrical pores due to the small cross section of the interfaces and so special attention was paid to the homogeneity of the fluids along the pore axis. We restricted our simulations of the coexisting densities to temperatures, where no exchange of identity between the simulation cells was observed. So, we determined two characteristic temperatures: T_L is the highest temperature, where coexistence of two different densities is surely observed; T_U is the temperature where two-phase coexistence was definitely absent. In the temperature interval between T_L and T_U exchange of the identities between the two simulation cells prevents a clear conclusion about the phase coexistence, based on the GEMC simulation. The critical density was estimated as the average density of the two coexisting phases at $T=T_L$.

C. Determination of two-phase coexistence from block density distribution

In the GEMC method the coexisting phases are simulated without explicit interface. Practically, in cylindrical pores phase separation occurs as a sequence of alternating domains of coexisting phases and therefore the absence of explicit interfaces in the Gibbs ensemble may lead to deviating results of corresponding simulations, especially when locating the pore critical temperature. In order to estimate this effect, we simulated water in a lengthy hydrophobic cylindrical pore ($U_0=-0.39$ kcal/mol, $R_P=12$ A, $L=300$ A, $N=794$). The average water density 0.218 g cm^{-3} was chosen close to the critical density, $\rho_C=0.235$ g cm^{-3}, estimated from the GEMC simulations. For the analysis, the pore was divided along the axis into 30 subsections (of 10 A length each) and the density distributions were extracted every 1000th MC move and averaged over 1×10^5 to 3×10^5 configurations for various temperatures.

III. RESULTS

A. Coexistence curve of bulk water

To test our techniques for the transfer of molecules, we simulated the liquid–vapor coexistence curve of bulk TIP4P water. The obtained liquid–vapor coexistence curve is presented in Fig. 5. For comparison the results of other simulations[71–75] are also shown. The deviations of our curve from the other results at high temperatures may be attributed mainly to different ratios of the numbers of water molecules in the coexisting phases. The use of essentially less mol-

ecules in the vapor phase in comparison with the liquid phase results in a shift of the top of the coexistence curves towards lower densities.[76]

Using our efficient techniques for the molecular transfers allowed us to achieve an essential number of successful transfers ($>10^4$) even at $T=125$ K. An extension of the coexistence curve in the supercooled region evidences a water density maximum around 250 K, in agreement with the results of NPT simulations of TIP4P water at low temperatures.[77,78] From 225 to 125 K the density of the liquid increases again. Below 125 K molecular transfers between vapor and liquid are still possible, but the time necessary for reliable equilibration increases drastically.

The melting temperature of model TIP4P ice is about 238 K.[79] In our simulations the dense water phase remains liquidlike or glasslike and does not show long-range order at all studied temperatures. We may assume, that at $T<238$ K this phase is metastable with respect to crystallization. Note, that freezing of bulk water in computer simulations was achieved recently, but at negative pressures,[80] whereas in our simulations supercooled water is in equilibrium with the vapor phase.

The critical parameters of the coexistence curve were estimated from a fit of the simulated data in the temperature interval above 300 K to extended scaling laws for the order parameter $\Delta\rho=(\rho_l-\rho_v)/2\rho_C$ and the diameter $(\rho_l+\rho_v)/2$,

$$\Delta\rho=B_0\tau^{\beta}(1+B_{\Delta}\tau^{\Delta}), \tag{4}$$

$$(\rho_l+\rho_v)/2=\rho_C(1+A_1\tau+A_2\tau^2), \tag{5}$$

where $\tau=(T_C-T)/T_C$. $\beta=0.326$ and $\Delta=0.5$ are the universal critical exponents for the Ising model. $B_0=2.33$, $B_{\Delta}=-0.24$, $A_1=1.58$, $A_2=-1.00$, $\rho_C=0.330\ \mathrm{g\,cm^{-3}}$, $T_C=580.2$ K are obtained from the fitting procedure.

B. Evolution of the coexistence curves of water with strengthening water–substrate interaction

The coexistence curves of water in cylindrical pores with radius $R_P=12$ A and various strengths of the water–substrate interaction are shown in Fig. 6. The critical parameters and the shape of the coexistence curves change drastically with strengthening water–substrate interaction. Moreover, at some level of pore hydrophilicity, the coexistence curve splits into two or three two-phase regions. In all studied systems the dense water phases remain liquidlike or glasslike even at the lowest temperatures, i.e., they do not show long-range order. As discussed above, we cannot exclude that these are metastable states with respect to crystallization.

In the hydrophobic pore ($U_0=-0.39$ kcal/mol, Fig. 6) the densities of the vapor and liquid phases of the single coexistence curve approach each other with increasing temperature faster than in the bulk case, mainly due to the decrease of the liquid phase density. For illustration, snapshots of the water molecules in the coexisting vapor and liquid phases in a hydrophobic ($U_0=-0.39$ kcal/mol) slitlike pore with $H_P=24$ A are shown in Fig. 7. This figure evidences, that the density of the liquid phase decreases with increasing temperature nonuniformly: the density in the surface layer

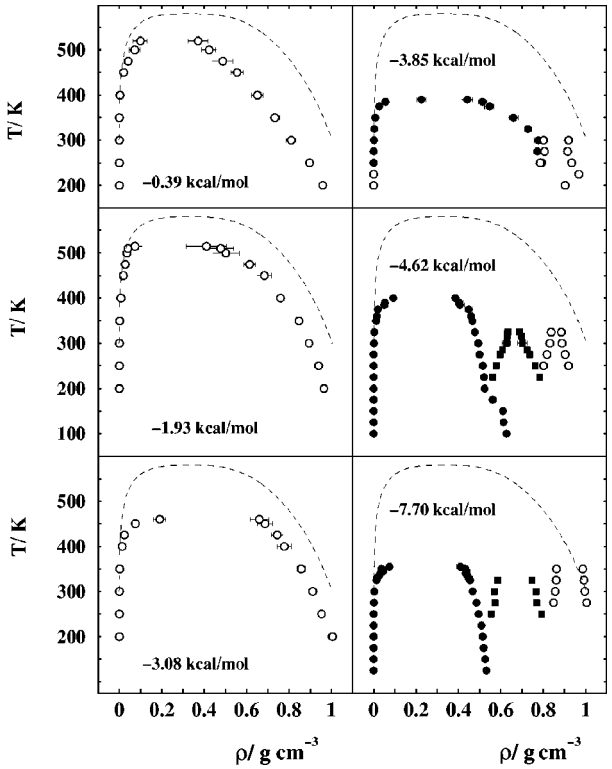

FIG. 6. Coexistence curves of water in cylindrical pores with radius $R_P=12$ A and various strengths of water–substrate interaction. The values of the interaction well depth U_0 are shown in the figure. The dashed curve represents the coexistence curve of bulk TIP4P water (Fig. 5).

decreases faster than in the pore center. A similar behavior for hydrophobic cylindrical pores was reported in our paper.[41]

Strengthening the water–substrate interaction from $U_0=-0.39$ kcal/mol to $U_0=-3.08$ kcal/mol does not cause the appearance of new phase transitions. The critical temperature T_C of the single liquid–vapor coexistence curve de-

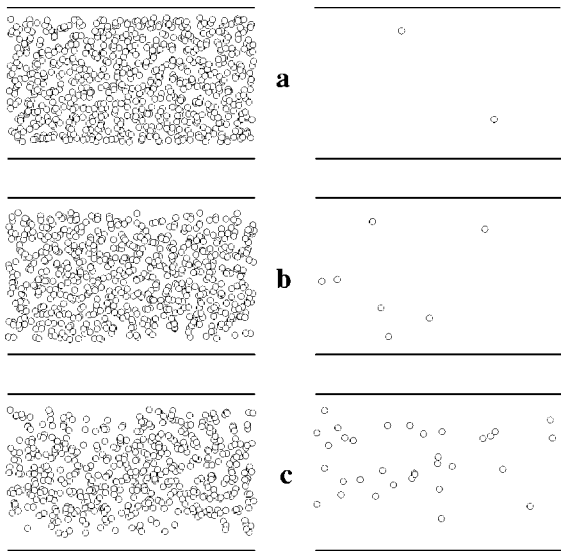

FIG. 7. Arrangement of the water oxygens in the coexisting liquid and vapor phases in a hydrophobic slitlike pore with $H_P=24$ A and $U_0=-0.39$ kcal/mol. (a) $T=200$ K; (b) $T=400$ K; (c) $T=530$ K.

TABLE I. Estimated critical parameters of water in pores. The critical temperature of each phase transition is located between T^L, the highest temperature where coexistence of two phases was observed, and T^U, the lowest temperature where mixing was observed during the GEMS runs. ρ_C is the mean value of the densities of the coexisting phases at $T=T^L$.

Transition	Pore size, A	U_0, kcal/mol	T^L, (K)	T^U, K	ρ_C, g cm^{-3}
		Cylindrical pores			
Liquid–vapor	$R_P=12$	−0.39	520	550	0.235(40)
Liquid–vapor	$R_P=12$	−1.93	515	525	0.243(66)
Liquid–vapor	$R_P=12$	−3.08	460	470	0.426(36)
Prewetting	$R_P=12$	−3.85	390	400	0.333(23)
Liquid–vapor, "inner" water			300	315	0.860(12)
First layering	$R_P=12$	−4.62	400	405	0.239(14)
Second layering			325	340	0.660(15)
Liquid–vapor, "inner" water			325	340	0.861(15)
First layering	$R_P=12$	−7.70	355	360	0.242(12)
Second layering			325	335	0.667(11)
Liquid–vapor, "inner" water			350	360	0.923(14)
Liquid–vapor	$R_P=15$	−0.39	525	545	0.195(12)
First layering	$R_P=15$	−4.62	400	405	0.193(15)
Second layering			300	320	0.643(35)
Liquid–vapor, "inner" water			350	360	0.919(74)
Liquid–vapor	$R_P=20$	−0.39	535	545	0.162(10)
First layering	$R_P=20$	−4.62	400	405	0.110 (7)
Liquid–vapor, "inner" water			480	485	0.794 (6)
		Slitlike pores			
Liquid–vapor	$H_P=24$	−0.39	535	545	0.187(22)
First layering	$H_P=24$	−4.62	395	400	0.123 (7)
Second layering			315	325	0.429 (6)
Liquid–vapor, "inner" water			450	460	0.736(20)

creases from about 535 K for $U_0=-0.39$ kcal/mol to about 465 K for $U_0=-3.08$ kcal/mol, while the critical density increases from $\rho_C\approx 0.24\ \mathrm{g\,cm^{-3}}$ to $\rho_C\approx 0.43\ \mathrm{g\,cm^{-3}}$, respectively (see Table I). These changes are accompanied by strong changes of the shape of the coexistence curve. The analysis of the water density profiles along the pore radius (Fig. 8) shows the appearance of two water layers near the pore wall. In the pores with U_0 lower than about −1.5 kcal/mol this layered structure remains pronounced in the liquid phase even at the highest temperature, at which the liquid–vapor coexistence was obtained. The flattening of the top of the coexistence curve with strengthening water–substrate interaction up to $U_0=-3.08$ kcal/mol, may be attributed to an approach of the system towards two dimensionality due to development of a layer structure of liquid water near the pore wall.[41]

At the water–pore interaction strength of $U_0=-3.85$ kcal/mol the coexistence curve splits into two coexistence regions (Fig. 6). Snapshots of the water molecules in the coexisting phases in such a pore (Fig. 9) show, that one of the transitions [pairs of solid circles in Fig. 6 at $T\geqslant 250$ K and snapshots in Fig. 9(a)] is a transition from vapor to a state, consisting mainly of two water layers near the pore wall and therefore it may be identified as a prewetting transition. Another transition [pairs of open circles in Fig. 6 at $T\geqslant 250$ K and snapshots in Fig. 9(b)] corresponds to a liquid–vapor phase transition in the interior of a pore with a wall, which is already covered by two water layers. In the low-temperature region ($T<250$ K) only liquid–vapor coex-

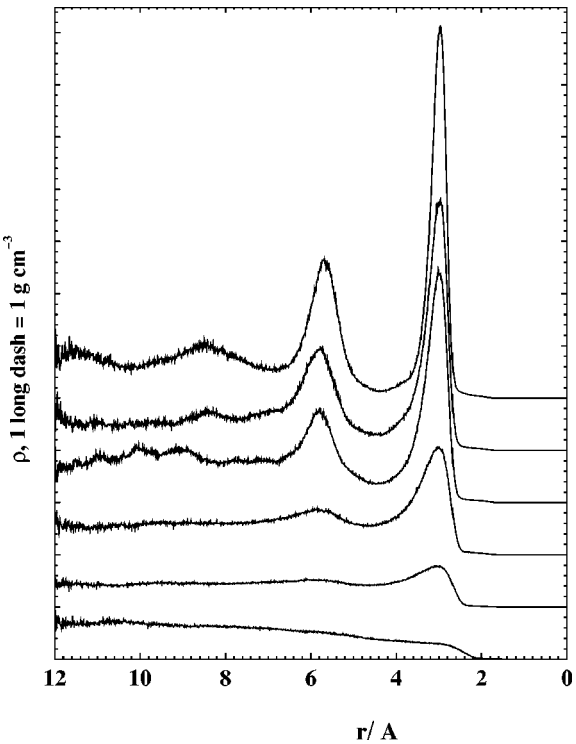

FIG. 8. Density profiles of the liquid–water phase in the cylindrical pores with $R_P=12$ A (highest density equilibrium line in Fig. 6). $r=0$, pore wall; $r=12$ A, pore center. The strength of the water–substrate interaction $|U_0|$ increases from bottom to the top and corresponds to the pores, shown in Fig. 6. These profiles were calculated for the highest temperature T^U where two-phase coexistence was observed in the simulations (see Table I).

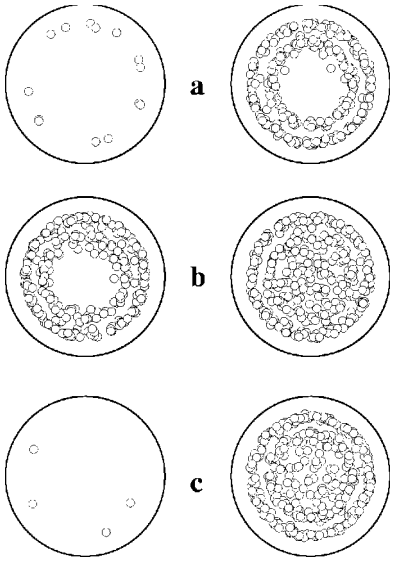

FIG. 9. Arrangement of the water oxygens in coexisting phases in the cylindrical pore with $R_P=12$ A and $U_0=-3.85$ kcal/mol (Fig. 6). (a) Prewetting transition at $T=250$ K; (b) liquid–vapor transition of ''inner'' water at $T=250$ K; (c) liquid–vapor transition at $T=200$ K.

istence was observed [Fig. 9(c)], that may suggest the existence of a triple point at $T\approx 250$ K and $\rho\approx 0.8\ \mathrm{g\,cm^{-3}}$, where vapor, water bilayer, and liquid phase coexist.

Further strengthening of the water–substrate interaction results in the appearance of three two-phase regions (Fig. 6, $U_0=-4.62$ kcal/mol and $U_0=-7.70$ kcal/mol). The origin of the observed three phase transitions in the hydrophilic pores is clearly seen from Fig. 10, where snapshots of water molecules in a slitlike pore with $U_0=-4.62$ kcal/mol are shown (similar figures were obtained also for cylindrical pores). The first and the second transitions in Fig. 6 correspond to the first [Fig. 10(a)] and second [Fig. 10(b)] layering transitions, respectively, i.e., to liquid–vapor transitions

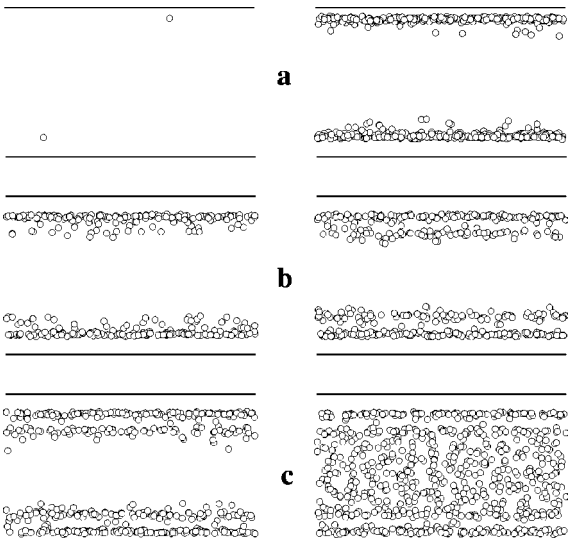

FIG. 10. Arrangement of water oxygens in coexisting phases in the hydrophilic slitlike pore with $H_P=24$ A and $U_0=-4.62$ kcal/mol. (a) First layering transition; (b) second layering transition; (c) liquid–vapor transition of the ''inner'' water.

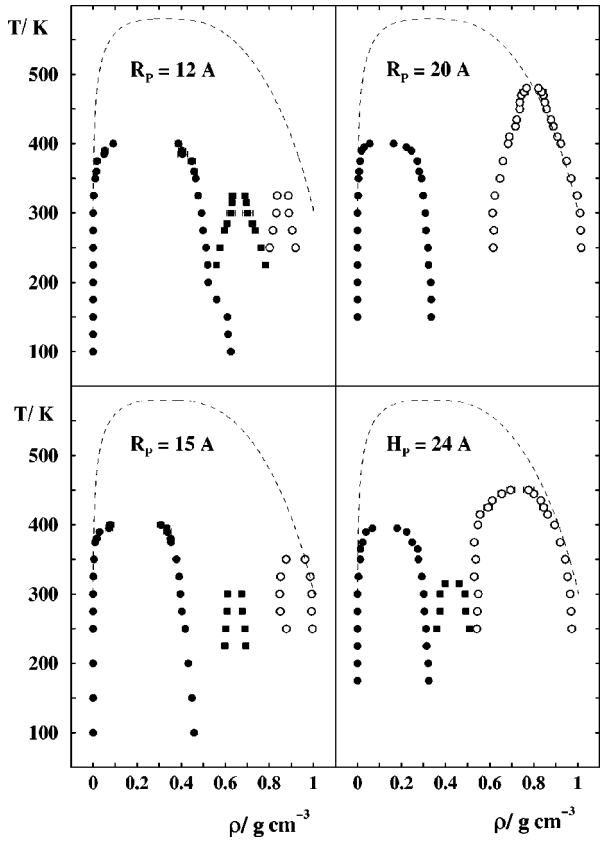

FIG. 11. Coexistence curves of water in hydrophilic pores with $U_0=-4.62$ kcal/mol. (a)–(c) cylindrical pores; (d) slitlike pore. Pore sizes are indicated in the figure.

of water in quasi-two-dimensional systems. The third transition corresponds to a liquid–vapor transition in the inner part of the pore [Fig. 10(c)]. The critical temperature of the first layering transition T_{L1} decreases from about 400 K to about 355 K, when the water–substrate interaction strengthens from $U_0=-4.62$ kcal/mol to $U_0=-7.70$ kcal/mol (see Fig. 6 and Table I).

The location of the second layering transition shows, that in a small hydrophilic pore (Fig. 6, $U_0=-4.62$ kcal/mol) there may exist a triple point with the first layering transition (in this case the one-layer phase of the first transition is metastable with respect to the denser phases at $T<200$ K), alternatively, the second layering transition may show re-entrant behavior.[81]

C. Coexistence curves of water in hydrophilic pores

When the size of the hydrophilic pore increases (Fig. 11), the coexistence region, which corresponds to the first layering transition, becomes narrower, simply due to the lower fraction of the water monolayer with respect to the total pore volume. The critical temperature of the first layering transition practically does not vary with changing pore size and shape (Fig. 11, Table I), but is sensitive to the strength of the water–substrate interaction (Fig. 6, Table I). The shape of the coexistence curve, which corresponds to the first layering transition, is close to the 2D Ising behavior[41] and will be discussed in more details in the subsequent paper.

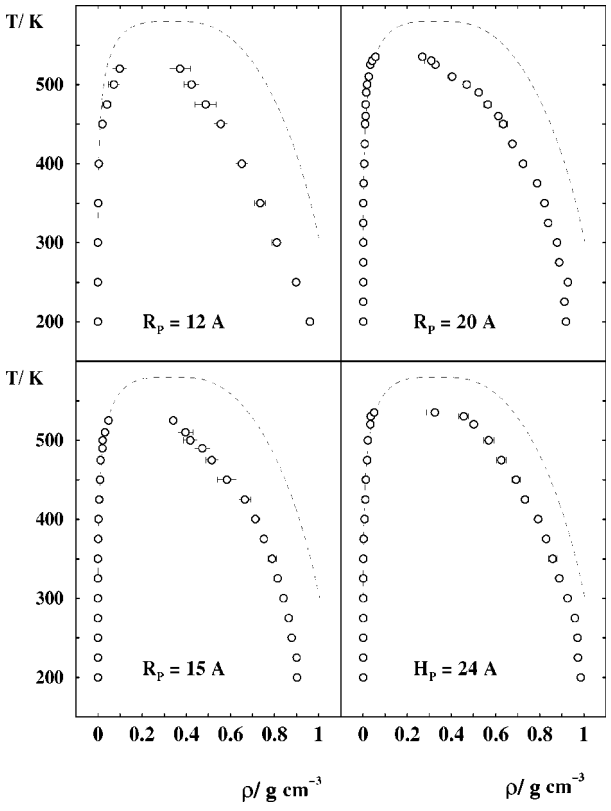

FIG. 12. Coexistence curves of water in hydrophobic pores with $U_0=-0.39$ kcal/mol. (a)–(c) cylindrical pores; (d) slitlike pore. Pore sizes are indicated in the figure.

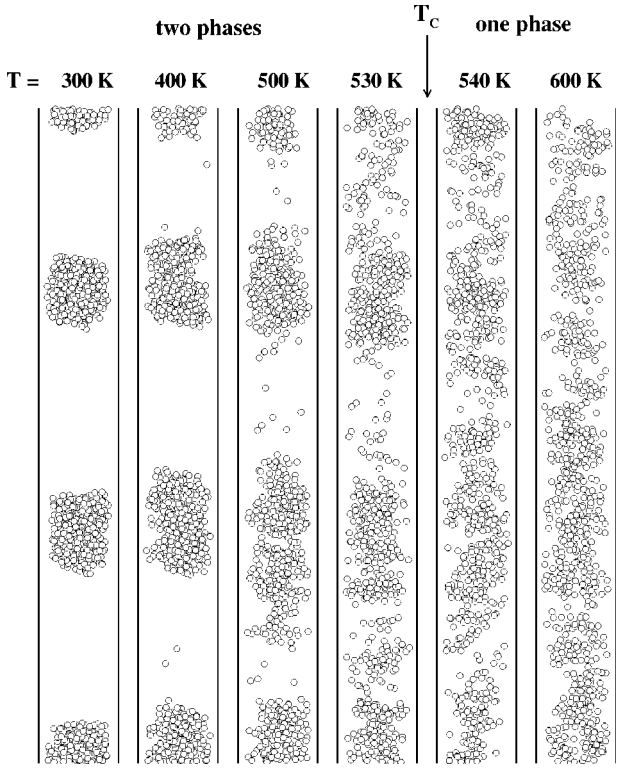

FIG. 13. Arrangement of water oxygens in a hydrophobic cylindrical pore with radius $R_P=12$ A, length $L=300$ A, $U_0=-0.39$ kcal/mol and average density $\rho_C=0.218$ g cm^{-3} at various temperatures.

The second layering transition shrinks and disappears with increasing radius of cylindrical pores. The shape of the corresponding coexistence curve cannot be analyzed. The liquid–vapor transition in the interior of the pore becomes dominant with increasing pore size: its critical temperature increases strongly (Fig. 11, Table I). In the narrow cylindrical pores ($R_P=12$ A and $R_P=15$ A) we can only approximately locate the corresponding two-phase region, whereas in the larger pores (cylindrical pore with $R_P=20$ A and slitlike pore with $H_P=24$ A) the liquid–vapor coexistence curves were obtained with essentially higher accuracy. Note the specific shapes of the coexistence curves in the two latter cases, which will be discussed in Sec. IV.

D. Coexistence curves of water in hydrophobic pores

In the hydrophobic pores the size has not such a strong effect on the coexistence curves (Fig. 12), as in the case of the hydrophilic pores. The pore critical temperature T_C for all four simulated hydrophobic pores is about 530–540 K, and a change with increasing pore size cannot be detected within the accuracy of our simulations. The estimated values of the critical density ρ_C in the hydrophobic pores are found essentially below the bulk value (Table I). In cylindrical pores ρ_C decreases with increasing pore radius (Table I). This effect cannot be explained by an ambiguous choice of the volume, occupied by the water in the pore. Probably it is connected with the estimation of the critical density as the average value of the densities of the coexisting phases at the highest observed temperature (see Sec. II B): in the larger pores it is possible to observe coexistence at higher temperature than in the smaller ones. Besides, different ratios of the numbers of molecules in the liquid and the vapor phases in different pores may also cause this effect.[76]

To check the reliability of the GEMC simulations, we performed a simulation of water in a lengthy hydrophobic pore ($U_0=-0.39$ kcal/mol, $R_P=12$ A, $L=300$ A) at an average density $\rho_C=0.218$ g cm^{-3} and different temperatures. Snapshots of the water molecule distribution in such a pore at various temperatures are shown in Fig. 13. Liquid and vapor domains are clearly seen at temperatures $T\leqslant 530$ K. With increasing temperature the interfaces between the domains become less pronounced and above some temperature (about the pore critical temperature T_C) the fluid structure becomes homogeneous along the pore axis. To locate the pore critical temperature more accurately we calculated the water density distributions, shown in Fig. 14. Distributions with one maximum, indicating a one-phase state, are observed at high temperatures, whereas distributions with two maxima, indicating a two-phase state, appear below a temperature of about 530–540 K, in good agreement with the results of the GEMC simulations (Fig. 12, Table I). Note, that due to the limited length of the simulation runs, the snapshots shown in Fig. 13 do not represent the equilibrium length of domains at low temperatures, which should be essentially longer.[21]

IV. DISCUSSION

The presented coexistence curves of bulk and confined water were obtained by Gibbs ensemble Monte Carlo

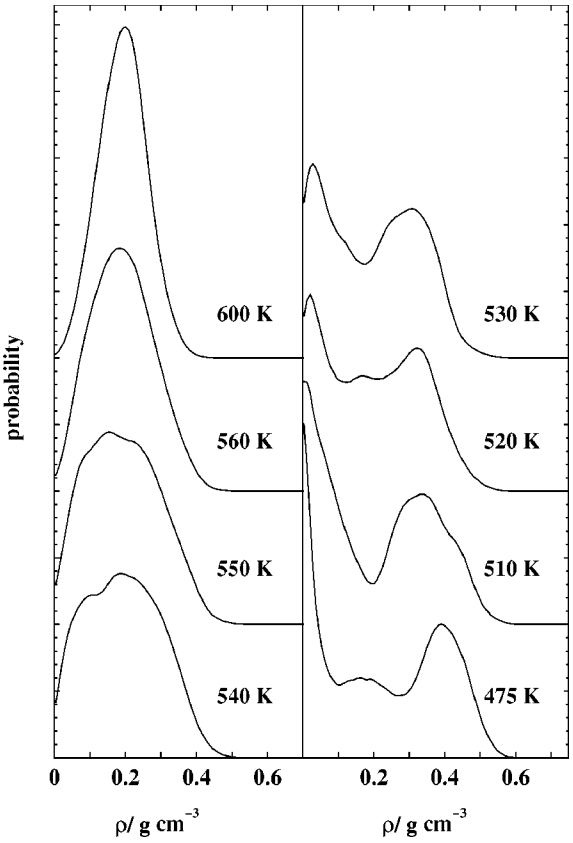

FIG. 14. Water density probability distributions in a hydrophobic cylindrical pore with radius $R_P=12$ A, length $L=300$ A, $U_0=-0.39$ kcal/mol and average density $\rho_C=0.218$ g cm^{-3} at various temperatures.

simulations,[57,62] which remains the most direct and accurate method to locate phase coexistence in a wide range of temperature and density. We used efficient techniques for molecular transfers, that essentially extend the applicability of the GEMC simulations towards denser phases and lower temperatures.[82–86] The reliability of these techniques was confirmed by calculations of the bulk water chemical potential. In addition, the densities in the vicinity of the density maximum near $T=250$ K, as obtained from our simulations of the bulk fluid coexistence curve, are in agreement with results from NPT ensemble simulations at atmospheric pressure.[77,78] Moreover, the pore critical temperature estimated from a GEMC simulation agrees with an estimation, obtained from block density distributions.

Our transfer techniques allowed to achieve extremely low temperatures (down to 125 K) of the simulated liquid–vapor coexistence of bulk water. A sufficient number of transfers between the vapor and the liquid phase in the Gibbs ensemble MC simulations provides a reliable sampling of the configurational space of (metastable) liquid water, which is unachievable by other methods (molecular dynamics or canonical MC ensembles). Therefore, the use of Gibbs ensemble MC simulations is a promising way to study supercooled liquids (for its application to low temperature ST2 water, see Ref. 87).

We have simulated coexistence curves of water in nanopores of different shapes, sizes, and strengths of water–substrate interaction. To our knowledge, this collection is the most detailed simulation study of the coexistence curves of a confined fluid. A large variety of coexistence curves is observed, in agreement with theoretical predictions of a rich phase behavior for confined fluids. The number of phase transitions in pores varies from a single liquid–vapor coexistence to three two-phase coexistence regions. Thus, from one to three critical points were found in nanopores. The nature of each observed phase transition was investigated by analyzing density distributions and snapshots of the molecular arrangements. We observed five kinds of phase transitions in pores: two kinds of ''bulklike'' liquid–vapor phase transitions (with a wall covered or not covered with two water layers) and three quasi-two-dimensional liquid–vapor surface transitions (first layering transition, second layering transition, and prewetting).

Generally, two-phase regions occupy the largest part of the density range at ambient and close to ambient temperatures, leaving little space for one phase states of the fluid. This means that the two-phase state is the most probable state of fluids in incompletely filled pores. In cylindrical pores and porous materials with low porosity, phase separation appears as alternating domains of two distinct coexisting phases and this is the most probable state of water at ambient temperatures. Variation of the degree of pore filling within the density range of a coexistence region causes a redistribution of the pore volume between the two phases only, without affecting the structure of each phase itself. This fact should be taken into account in the treatment of experimental data obtained in partially filled pores, where usually a one-phase state is assumed, i.e., that the pore wall is covered homogeneously by a liquid film with a thickness, estimated from the level of pore filling.[88] Such an assumption may cause apparent contradictions in the treatment of experimental data.[89] A dominance of two-phase coexistence over one-phase states indicates that MC (or MD) simulations performed for incompletely filled pores[90] may frequently deal with states in the two-phase regions or with unstable states. The simulation of unstable states is quite possible if the separation of the fluid into two phases is hampered by a small system size and/or a short time of simulation.

A one-phase state of a confined fluid, usually vapor or liquid, is observed in equilibrium with a saturated bulk. The vapor state is observed in weakly attractive pores (capillary evaporation), whereas the liquid state is observed in strongly attractive pores (capillary condensation).[82–84,91] It was shown, that capillary condensation of water occurs in cylindrical pores with radius $R_P=12$ A, when the water–substrate interaction is stronger than $U_0\approx-1.0$ kcal/mol.[84] Among the pores, analyzed in the present paper, all pores with $U_0=-0.39$ kcal/mol are expected to show capillary evaporation in equilibrium with bulk water. Only one coexistence region (liquid–vapor) is observed in such pores. All other considered pores show capillary condensation[84] and one, two or three phase transitions are observed. The most typical porous materials studied experimentally show capillary condensation, and so the possibility of multiple phase transitions should be taken into account for a correct interpretation of the experimental data. Note the recent experi-

mental indications on the possibility of two fluid–fluid transitions of nitrogen in cylindrical pores.[9]

Only one transition (liquid–vapor) is observed in the pores with weak and moderate strength of water–substrate interaction ($U_0=-0.39$ kcal/mol, $U_0=-1.93$ kcal/mol, and $U_0=-3.08$ kcal/mol, see Fig. 6). The shift ΔT_C of the critical temperature in these pores with respect to the bulk value T_{3D} varies from $0.07T_{3D}$ to $0.20T_{3D}$ in this range of a water–substrate interaction. This means, that ΔT_C may increase by a factor of 3 due to a strengthening water–substrate interaction, in agreement with theoretical estimations.[29] Note, that a further weakening of the water-substrate interaction by adding a repulsive step near the pore wall does not influence significantly the critical temperature and leads to the formation of an additional transition in the high-density region of the phase diagram.[85]

Surface transitions split from the main liquid–vapor coexistence curve when the strength of the fluid–substrate interaction becomes close to the typical strength of the pair interaction in the fluid. This qualitatively agrees with experimentally observed changes of the pore condensation process due to modifications of the pore surface.[92] We found one or two surface transitions, depending on pore size and fluid–substrate interaction. The most typical surface transition obtained in our simulations is the first layering transition, when phase coexistence occurs between vapor and a single liquid layer at the pore wall (close to a two-dimensional condensation). The apparent shape of the coexistence curves, which correspond to the first layering transition, is close to the 2D Ising model, as expected for all surface transitions.[35] The critical temperature of the first layering transition is about $T_{L1}\approx 0.69T_{3D}$ at $U_0=-4.62$ kcal/mol and is *not* sensitive to variations of pore size and shape (see Fig. 11, Table I). Strengthening the water–substrate interaction to $U_0=-7.70$ kcal/mol (Fig. 6) depresses the critical temperature to $T_{L1}\approx 0.62T_{3D}$.

The lower limit for T_{L1} was estimated by simulating a quasi-two-dimensional system, where all oxygens were placed in one plane, while molecular rotations were not restricted.[93] The critical temperature of the liquid–vapor phase transition in such a system was found at $T_{2D}\approx 0.57T_{3D}$ and corresponds to the layering transition on a substrate with infinite attraction ($U_0\rightarrow-\infty$). So, the possible temperature interval for the critical temperature of the first layering transition of water on a smooth substrate we estimate as $0.57T_{3D}<T_{L1}<0.69T_{3D}$. Experimental estimates of the critical temperature of two-dimensional condensation of water on strongly attractive substrates give values from $0.36T_{3D}$ to values larger than $0.47T_{3D}$.[94] The higher value of T_{2D}, obtained in our simulations, may be due to the free molecular rotations, which are not restricted by the substrate in our model. For comparison, in simulated LJ systems $T_{2D}\approx 0.38T_{3D}$.[95] This is in good agreement with $0.38T_{3D}<T_{L1}<0.55T_{3D}$, obtained experimentally for quasi-two-dimensional condensation of noble gases on strongly attractive substrates.[96]

The second layering transition is a quasi-two-dimensional one of water on a substrate, which is already covered by one liquid layer. It occurs in a much smaller density range, then the first layering transition. In cylindrical pores there is an obvious geometrical reason for such an effect: the fraction of molecules in a layer depends on its distance from the pore axis. However, the phase diagram for the slitlike pore (Fig. 11) and the density profiles (Fig. 8) show an additional reason: the local density in the second layer is significantly lower, then in the first one. The critical temperature of the second layering transition T_{L2} is always lower then the critical temperature of the first layering transition T_{L1} and is located between $T_{L2}\approx 0.54T_{3D}$ and $0.59T_{3D}$. A similar behavior was found by density functional calculations for a strongly associative LJ fluid in pores.[44] The second layering transition is considerably influenced by the pore size and shape. In cylindrical pores with $U_0=-4.62$ kcal/mol it shrinks with increasing pore radius and finally disappears at $R_P=20$ A (see Fig. 11).

In our simulations we never observed a third layering transition of confined water and we do not expect its appearance even with strengthening water–substrate interaction or increasing pore size. The reason for this conjecture is, that near the wall of the hydrophilic pores there are two pronounced water layers, whereas deeper inside, the density distribution is almost homogeneous even in strongly hydrophilic pores (see Fig. 8). The structuring of a first layer allows sometimes stabilization of a second layer, whereas the second layer never provides stabilization of a third layer in the considered range of water–substrate interactions (see Ref. 82 for the details of water structure in surface layers). The existence of one to three specific water layers near the substrate, so-called bound water, was reported in various experimental studies of water in pores[97–100] and was confirmed by computer simulations.[82–84]

A prewetting transition, the simultaneous condensation of two water layers, is observed when the strength of the fluid–substrate interaction is comparable to the molecular pair interaction in the fluid [Figs. 6 and 9(a) for $U_0=-3.85$ kcal/mol]. It persists in a wide temperature range between the critical temperature at about $0.68T_{3D}$ and the triple point at about $0.43T_{3D}$. The observation of a prewetting transition with a triple point agrees with theoretical predictions[28] and lattice gas simulations.[101]

In hydrophilic pores a liquid–vapor phase transition of the ''inner'' water occurs in a pore with a wall, which is already covered by two liquid water layers [see Figs. 6, 9(b), and 10(c)]. The density interval of this transition increases with increasing pores size and it becomes dominant in large pores (Fig. 11, open circles). Structured surfaces of real pores may effect strongly the surface transitions, but much less the phase transition of the ''inner'' water, which seems to be the most prominent transition in real porous materials. Indeed, experimental studies of water freezing in incompletely filled pores evidence the coexistence of two phases, namely a fluid film (of one to two water layers) and a liquid.[100]

The critical temperature of the phase transition of the ''inner'' water is highly sensitive to the pore size. In the cylindrical pores with $U=-4.62$ kcal/mol, it varies from about $0.58T_{3D}$ to $0.83T_{3D}$, when the pore radius R_P increases from 12 A to 20 A. Such a strong size effect and the

almost homogeneous density of the ''inner'' water (see Fig. 8) make this system a good candidate to test theoretical predictions[14,27–29] concerning the effect of finite size on the critical temperature. Such simulations are in progress now.

This liquid–vapor phase transition of the ''inner'' water in narrow pores can be located only approximately and the shape of the coexistence curve may be analyzed only for the two largest of the examined hydrophilic pores (see Fig. 11). There is a surprising resemblance between the simulated coexistence curve of the ''inner'' water in the cylindrical pore with $R_P = 20$ A and the few available experimentally estimated coexistence curves of fluids in pores with dominating cylindrical geometry (see Fig. 6 of Ref. 2 and Fig. 7 of Ref. 4). Not only the location of the coexistence curve of the confined fluid with respect to the bulk, but also the shape of the coexistence curves are similar. Attempts to fit such curves to a scaling law will give an effective value of the critical exponent β higher than the 3D Ising value $\beta = 0.326$. The bottlelike shape of the simulated coexistence curve of the ''inner'' water is in agreement with experimental results obtained for helium in aerogels.[1] The bottlelike shape of the coexistence curve may be connected with the formation of a wetting layer in the vapor phase. Moreover, it may also be influenced by a temperature induced change of the surface water layers. This hypothesis can be checked by an analysis of the local density distributions at various temperatures and will be presented in our next paper.

An intriguing result was obtained for the liquid–vapor phase transition in hydrophobic pores. The pore critical temperature is about $0.92T_{3D}$ to $0.93T_{3D}$ for the considered pores, despite an essential variation of their size. Obviously, an analysis of the size effect on the critical temperature requires simulations of hydrophobic pores in a wider range of pore sizes and these simulations are in progress. All coexistence curves, shown in Fig. 12, look very similar and show a strong decrease of the density in the liquid phase with increasing temperature. This is connected with the specific behavior of the surface layer, which in a wide temperature range has a density which is essentially lower than the water density in the pore interior (see Fig. 8). This effect strongly enhances with temperature. As discussed before,[41] this behavior of the confined fluid is very similar to the so-called ordinary surface transition, observed for the surface layers in lattice models.[37]

The properties of confined fluids are intimately related with the occurring spatial density variations. Density variations normal to the pore wall are observed in all possible phase states of water in pores. In hydrophilic pores water shows two highly structured layers near the pore wall with essentially lowered diffusivity in comparison with the bulk.[82,83] Additionally, the formation of a wetting layer in the vapor phase with increasing temperature causes a strong density gradient normal to the pore wall. In a hydrophobic pore the density of the liquid phase decreases towards the pore wall and this effect strongly increases with temperature. In addition to these density variations normal to the wall strong heterogeneities along the pore axis may occur in incompletely filled pores due to phase separation. This effect is especially important for cylindrical pores and other porous materials, where phase separation leads to the formation of alternating domains of the two coexisting phases. The presence of interfaces between the domains of the coexisting phases may also strongly influence water structure and dynamics at high temperatures, when the concentration of interfaces drastically increases. These inhomogeneities of the fluid, both along and normal to the pore axis, must be considered for a correct analysis of experimental results or computer simulations. The knowledge of the possible phase states of confined fluids and their densities at coexistences is a necessary prerequisite for the simulation of any property of confined water. The coexistence curves of water in nanopores, presented here, are intended to furnish a firm basis for such studies.

ACKNOWLEDGMENTS

This work was supported by Deutsche Forschungsgemeinschaft and by the Ministerium fur Schule und Weiterbildung, Wissenschaft und Forschung des Landes Nordrhein-Westfalen. The authors thank G. H. Findenegg for permanent interest to our work and many fruitful discussions, S. Dietrich and R. Evans for useful advices, and M. H. W. Chan for discussions and sending unpublished experimental results.

[1] A. P. Y. Wong and M. H. W. Chan, Phys. Rev. Lett. **65**, 2567 (1990); M. H. W. Chan, Czech. J. Phys. **46**, Suppl. S6, 2915 (1996); P. A. Wong, Ph.D. thesis, Pennsylvania State University, 1992.
[2] S. Gross and G. H. Findenegg, Ber. Bunsenges. Phys. Chem. **101**, 1726 (1991).
[3] A. P. Y. Wong, S. B. Kim, W. I. Goldburg, and M. H. W. Chan, Phys. Rev. Lett. **70**, 954 (1993).
[4] M. Tommes and G. H. Findenegg, Langmuir **10**, 4270 (1994).
[5] T. Herman and J. Beamish, J. Low Temp. Phys. **261**, 661 (2002).
[6] W. D. Machin, Phys. Chem. Chem. Phys. **5**, 203 (2003).
[7] C. G. V. Burgess, D. H. Everett, and S. Nuttall, Pure Appl. Chem. **61**, 1845 (1989).
[8] W. D. Machin, Langmuir **15**, 169 (1999).
[9] K. Morishige, H. Fujii, M. Uga, and D. Kinukawa, Langmuir **13**, 3494 (1997); K. Morishige and M. Shikimi, J. Chem. Phys. **108**, 7821 (1998); K. Morishige and M. Ito, *ibid.* **117**, 8036 (2002).
[10] E. Kierlik, M. L. Rosinberg, G. Tarjus, and P. Viot, Phys. Chem. Chem. Phys. **3**, 1201 (2001).
[11] R. Evans, J. Phys.: Condens. Matter **46**, 8989 (1990).
[12] A. V. Neimark, P. I. Ravikovitch, and A. Vishnyakov, Phys. Rev. E **62**, R1493 (2000).
[13] C. G. Sonwane, S. K. Bhatia, and N. Calos, Ind. Eng. Chem. Res. **47**, 2271 (1998).
[14] M. E. Fisher and H. Nakanishi, J. Chem. Phys. **75**, 5857 (1981).
[15] P. Tarazona, U. Marini Bettolo Marconi, and R. Evans, Mol. Phys. **60**, 573 (1987).
[16] V. Privman and L. S. Schulman, J. Phys. A **15**, L231 (1982).
[17] G. S. Heffelfinger, F. Swol, and K. E. Gubbins, Mol. Phys. **61**, 1381 (1987); J. Chem. Phys. **89**, 5202 (1988).
[18] B. K. Peterson, K. E. Gubbins, G. S. Heffelfinger, U. Marini Bettolo Marconi, and F. Swol, J. Chem. Phys. **88**, 6487 (1988).
[19] C. Bichara, J. Y. Raty, and R. J.-M. Pellenq, Phys. Rev. Lett. **89**, 016101 (2002).
[20] V. Privman and M. E. Fisher, J. Stat. Phys. **33**, 385 (1983).
[21] L. D. Gelb and K. E. Gubbins, Phys. Rev. E **55**, R1290 (1997); **56**, 3185 (1997).
[22] Z. Zhang and A. Chakrabarti, Phys. Rev. E **50**, R4290 (1994).
[23] R. Valiullin and I. Furo, J. Chem. Phys. **116**, 1072 (2002).
[24] F. Brochard and P. G. de Gennes, J. Phys. (France) Lett. **44**, 785 (1983); P. G. de Gennes, J. Phys. Chem. **88**, 6469 (1984).
[25] W. T. Thomson, Philos. Mag. **42**, 448 (1871).
[26] M. E. Fisher and A. N. Berker, Phys. Rev. B **26**, 2507 (1982).

[27] R. Evans, U. Marini Bettolo Marconi, and P. Tarazona, J. Chem. Phys. **84**, 2376 (1986).
[28] R. Evans, U. Marini Bettolo Marconi, P. Tarazona, J. Chem. Soc., Faraday Trans. 2 **82**, 1763 (1986).
[29] H. Nakanishi and M. E. Fisher, J. Chem. Phys. **78**, 3279 (1983).
[30] J. W. Cahn, J. Chem. Phys. **66**, 3667 (1977).
[31] H. Nakanishi and M. E. Fisher, Phys. Rev. Lett. **49**, 1565 (1982).
[32] S. Dietrich, in *Phase Transitions and Critical Phenomena*, edited by C. Domb and J. L. Lebowitz (Academic, New York, 1988), Vol. XII, p. 1.
[33] E. Bruno, U. Marini Bettolo Marconi, and R. Evans, Physica A **141**, 187 (1987).
[34] P. C. Ball and R. Evans, J. Chem. Phys. **89**, 4412 (1988).
[35] D. Nicolaides and R. Evans, Phys. Rev. Lett. **63**, 778 (1989).
[36] K. Binder and D. Landau, J. Chem. Phys. **96**, 1444 (1992).
[37] K. Binder, in *Phase Transitions and Critical Phenomena*, edited by C. Domb and J. Lebowitz (Academic, London, 1983), Vol. 8, p. 1.
[38] T. W. Burkhardt and H. W. Diehl, Phys. Rev. B **50**, 3894 (1994).
[39] L. Sigl and W. Fenzl, Phys. Rev. Lett. **57**, 2191 (1986); W. Fenzl, Europhys. Lett. **24**, 557 (1993).
[40] B. M. Law, Prog. Surf. Sci. **66**, 159 (2001).
[41] I. Brovchenko, A. Geiger, and A. Oleinikova, Phys. Chem. Chem. Phys. **3**, 1567 (2001).
[42] L. D. Gelb, K. E. Gubbins, R. Radhakrishnan, and M. Sliwinska-Bartkowiak, Rep. Prog. Phys. **62**, 1573 (1999).
[43] A. Huerta, S. Sokolowski, and O. Pizio, Mol. Phys. **97**, 919 (1999).
[44] A. Huerta, O. Pizio, and S. Sokolowski, J. Chem. Phys. **112**, 4286 (2000).
[45] B. M. Malo, L. Salazar, S. Sokolowski, and O. Pizio, J. Phys.: Condens. Matter **12**, 8785 (2000).
[46] M. Schoen and D. J. Diestler, J. Chem. Phys. **109**, 5596 (1998).
[47] E. Kierlik, M.-L. Rosinberg, G. Tarjus, and P. A. Monson, J. Phys.: Condens. Matter **8**, 9621 (1996); J. Chem. Phys. **106**, 264 (1997).
[48] V. Krakoviack, E. Kierlik, M.-L. Rosinberg, and G. Tarjus, J. Chem. Phys. **115**, 11289 (2001).
[49] R. Radhakrishnan and K. E. Gubbins, Phys. Rev. Lett. **79**, 2847 (1997).
[50] K. S. Page and P. A. Monson, Phys. Rev. E **54**, R29 (1996); **54**, 6557 (1996).
[51] L. Sarkisov and P. A. Monson, Phys. Rev. E **61**, 7231 (2000).
[52] C. Saravana and S. M. Auerbach, J. Chem. Phys. **109**, 8755 (1998).
[53] A. V. Neimark and A. Vishnyakov, Phys. Rev. E **62**, 4611 (2000).
[54] M. Alvarez, D. Levesque, and J.-J. Weis, Phys. Rev. E **60**, 5495 (1999).
[55] W. Shi, X. Zhao, and J. K. Johnson, Mol. Phys. **100**, 2139 (2002).
[56] M. Rovere, D. W. Hermann, and K. Binder, J. Phys.: Condens. Matter **2**, 7032 (1990).
[57] A. Z. Panagiotopoulos, Mol. Phys. **62**, 701 (1987).
[58] A. M. Vishnyakov, E. M. Piotrovskaya, E. N. Brodskaya, E. V. Votyakov, and Yu. K. Tovbin, Russ. J. Phys. Chem. **74**, 162 (2000); Langmuir **17**, 4451 (2001).
[59] J. K. Brennan and W. Dong, J. Chem. Phys. **116**, 8948 (2002).
[60] K. Yasuoka, G. T. Gao, and X. C. Zeng, J. Chem. Phys. **112**, 4279 (2000).
[61] W. L. Jorgensen, J. Chandrasekhar, and J. D. Madura, J. Chem. Phys. **79**, 926 (1983).
[62] A. Z. Panagiotopoulos, Mol. Phys. **61**, 813 (1987).
[63] C. H. Bennett, J. Comput. Phys. **22**, 245 (1976).
[64] K. S. Singh and K. E. Gubbins, Mol. Phys. **46**, 1109 (1982).
[65] J. Hermans, A. Pathiaseril, and A. Anderson, J. Am. Chem. Soc. **110**, 5982 (1988).
[66] W. L. Jorgensen, J. F. Blake, and J. K. Buchner, Chem. Phys. **129**, 193 (1989).
[67] Z. Li and H. A. Sheraga, Chem. Phys. Lett. **154**, 516 (1989).
[68] B. Jayaram and D. L. Beveridge, J. Phys. Chem. **94**, 7288 (1990).
[69] M. Mezei, J. Comput. Chem. **13**, 651 (1992).
[70] S. D. Hong, B. J. Yoon, and M. S. Jhon, Chem. Phys. Lett. **188**, 299 (1992).
[71] J. J. de Pablo and J. M. Prausnitz, Fluid Phase Equilib. **53**, 177 (1989).
[72] R. F. Cracknell, D. Nicholson, N. G. Parsonage, and H. Evans, Mol. Phys. **71**, 931 (1990).
[73] M. J. Vlot, J. Huinik, and J. P. van der Eerden, J. Chem. Phys. **110**, 55 (1999).
[74] J. Vorholz, V. I. Harismiadis, B. Rumpf, A. Z. Panagiotopoulos, and G. Maurer, Fluid Phase Equilib. **170**, 203 (2000).
[75] M. Lisal, W. R. Smith, and I. Nezbeda, Fluid Phase Equilib. **181**, 127 (2001).
[76] J. P. Valleau, J. Chem. Phys. **108**, 2962 (1998).
[77] P. H. Poole, F. Sciortino, U. Essmann, and H. E. Stanley, Phys. Rev. E **48**, 3799 (1993).
[78] H. Tanaka, J. Chem. Phys. **105**, 5099 (1996).
[79] G. T. Gao, X. C. Zeng, and H. Tanaka, J. Chem. Phys. **112**, 8534 (2000).
[80] M. Matsumoto, S. Saito, and I. Ohmine, Nature (London) **416**, 409 (2002).
[81] A. Prasad and P. B. Weichman, Phys. Rev. B **57**, 4900 (1998).
[82] I. Brovchenko, D. Paschek, and A. Geiger, J. Chem. Phys. **113**, 5026 (2000).
[83] I. Brovchenko, A. Geiger, and D. Paschek, Fluid Phase Equilib. **183–184**, 331 (2001).
[84] I. Brovchenko and A. Geiger, J. Mol. Liq. **96–97**, 195 (2002).
[85] I. Brovchenko, A. Geiger, and A. Oleinikova, in *New Kinds of Phase Transitions: Transformations in Disordered Substances*, edited by V. V. Brazshkin, S. V. Buldyrev, V. N. Ryshov, and H. E. Stanley (Kluwer Academic, Berlin, 2002), pp. 367–380.
[86] I. Brovchenko and B. Guillot, Fluid Phase Equilib. **183–184**, 311 (2001).
[87] I. Brovchenko, A. Geiger, and A. Oleinikova, J. Chem. Phys. **118**, 9473 (2003).
[88] M.-C. Bellisent-Funel, J. Phys.: Condens. Matter **13**, 9165 (2001).
[89] J. Dore, Chem. Phys. **258**, 327 (2000).
[90] P. Gallo, M. Rovere, M. A. Ricci, C. Harting, and E. Spohr, Philos. Mag. B **79**, 1923 (1999); E. Spohr, C. Harting, P. Gallo, and M. Rovere, J. Mol. Liq. **80**, 165 (1999); P. Gallo, Phys. Chem. Chem. Phys. **2**, 1607 (2000); C. Harting, W. Witschel, E. Spohr, P. Gallo, M. A. Ricci, and M. Rovere, J. Mol. Liq. **85**, 127 (2000); P. Gallo, M. Rovere, and E. Spohr, J. Chem. Phys. **113**, 11324 (2000); F. Venturini, P. Gallo, M. A. Ricci, A. R. Bizzarri, and S. Cannistraro, Philos. Mag. B **82**, 507 (2002); P. Gallo, M. Rapinesi, and M. Rovere, J. Chem. Phys. **117**, 369 (2002).
[91] P. B. Balbuena and K. E. Gubbins, Langmuir **9**, 1801 (1993).
[92] A. Schreiber, H. Bock, M. Schoen, and G. H. Findenegg, Mol. Phys. **100**, 2097 (2002).
[93] I. Brovchenko, A. Geiger, and A. Oleinikova (unpublished).
[94] K. Morishige, S. Kittaka, and T. Morimoto, Surf. Sci. **109**, 291 (1981); **120**, 223 (1982).
[95] S. Jiang and K. E. Gubbins, Mol. Phys. **86**, 599 (1995).
[96] F. Millot, Y. Larher, and C. Tessier, J. Chem. Phys. **76**, 3327 (1982).
[97] K. Overloop and L. Van Gerven, J. Magn. Reson., Ser. A **101**, 179 (1993).
[98] E. W. Hansen, M. Stocker, and R. Schmidt, J. Phys. Chem. **100**, 2195 (1996); E. W. Hansen, E. Tangstad, E. Myrvold, and T. Myrstad, *ibid.* **101**, 10709 (1997).
[99] K. Morishige and K. Nobuoka, J. Chem. Phys. **107**, 6965 (1997); K. Morishige and K. Kawano, *ibid.* **110**, 4867 (1999).
[100] A. Schreiber, I. Ketelsen, and G. H. Findenegg, Phys. Chem. Chem. Phys. **3**, 1185 (2001).
[101] D. Nicolaides and R. Evans, Phys. Rev. B **39**, 9336 (1989).